

RSC Advances

Accepted Manuscript



This article can be cited before page numbers have been issued, to do this please use: D. Zákutná, I. Matulkova, E. Kentzinger, R. Medlín, Y. Su, K. Nemkovski, S. Disch, J. Vejpravova and D. Niznansky, *RSC Adv.*, 2016, DOI: 10.1039/C6RA21377D.



This is an Accepted Manuscript, which has been through the Royal Society of Chemistry peer review process and has been accepted for publication.

Accepted Manuscripts are published online shortly after acceptance, before technical editing, formatting and proof reading. Using this free service, authors can make their results available to the community, in citable form, before we publish the edited article. We will replace this Accepted Manuscript with the edited and formatted Advance Article as soon as it is available.

You can find more information about Accepted Manuscripts in the [author guidelines](#).

Please note that technical editing may introduce minor changes to the text and/or graphics, which may alter content. The journal's standard [Terms & Conditions](#) and the ethical guidelines, outlined in our [author and reviewer resource centre](#), still apply. In no event shall the Royal Society of Chemistry be held responsible for any errors or omissions in this Accepted Manuscript or any consequences arising from the use of any information it contains.

Dispersible Cobalt Chromite Nanoparticles: Facile Synthesis and Size Driven Collapse of Magnetism

View Article Online
DOI: 10.1039/C6RA21377D

D. Zakutna^{1,2,*†}, I. Matulkova¹, E. Kentzinger³, R. Medlin⁴, Y. Su⁵, K. Nemkovski⁵, S. Disch⁶, J. Vejpravova^{1,7,*‡}, D. Niznansky^{1,‡}

¹Department of Inorganic Chemistry, Faculty of Science, Charles University in Prague, Hlavova 2030/8, 12843 Prague 2, Czech Republic

²Structural and System Diagnostics, Research Centre Rez s.r.o., Hlavní 130, 25068 Husinec - Rez, Czech Republic

³Jülich Center for Neutron Sciences JCNS and Peter Grünberg Institute PGI, JARA-FIT, Forschungszentrum Jülich GmbH, 52425 Jülich, Germany

⁴New Technology Research Centre, University of West Bohemia, Univerzitní 8, 306 14 Pilsen

⁵Jülich Center for Neutron Sciences JCNS at Heinz Maier-Leibnitz Zentrum MLZ, Forschungszentrum Jülich GmbH, Lichtenbergstrasse 1, D-85747 Garching, München, Germany

⁶Department Chemie, Universität zu Köln, Luxemburger Strasse 116, 50939 Köln, Germany

⁷Department of Magnetic Nanosystems, Institute of Physics CAS, v.v.i., Na Slovance 2, 18221 Prague 8, Czech Republic

Multiferroic oxides have enormous application potential thanks to the mutually coupled magnetic and dielectric response embedded in a standalone material. Among them, the unique case is the cobalt chromite with spin-induced electric polarization locked to the magnetization direction and propagation vector of the spiral magnetic phase. The nature of the ground state magnetic structure gives rise to complex size dependent magnetic behaviour, which collapses when reaching a critical particle size. In our work, we focused on preparation of standalone cobalt chromite nanoparticles (NPs). We introduced hydrothermal decomposition of cobalt(II)/chromium(III) oleates in water/ethanol system without need of additional thermal treatment, which lead to stable cobalt chromite nanoparticles with diameter of 3.0(1) – 4.2(1) nm and log normal size distribution of 12 -16%. The size at the edge of the critical limit was tuned by the reaction temperature reaching typically 240±10 °C. The as-prepared NPs are coated with covalently bonded oleic acid and can be easily dispersed in non-polar solvents, which makes them excellent candidates for custom surface modifications. The NPs were studied using large number of characterization techniques: powder x-ray diffraction, transmission electron microscopy, small-angle x-ray scattering, and vibrational spectroscopies. The impact of size effect on magnetic properties was also investigated by temperature and magnetic field dependent magnetization, a.c. susceptibility and diffuse neutron scattering. The onset of collective glassy state due to the collapse of long range conical magnetic order was observed. The uniform cobalt chromite NPs coated with oleic acid with size of 3 - 4 nm are excellent prototypes for studying the size effect on magnetic (and ferroic), and can be subjected to manifold surface functionalization required for their embedding in smart nanostructures and nanocomposites.

1. Introduction

View Article Online
DOI: 10.1039/C6RA21377D

Nanoparticles (NPs) carrying intrinsic magnetic moments have been intensively investigated due to various applications, where the biomedicine and magnetic recording are the most significant^{1,2}. With decreasing particle size, the so-called single-domain state, which is a simple consequence of magneto-static to domain wall energy gain governs the magnetic properties of NPs. Consequently, such NPs exhibit superparamagnetic properties at temperatures and magnetic fields high enough to exceed the energy threshold for coherent rotation of the single-particle magnetization. The most prominent magnetic materials studied in the form of NPs are the spinel oxides, especially the ferrites. These materials have attracted significant attention mainly for their biocompatibility hand in hand with convenient magnetic properties making them excellent candidates for use in data storage media, dynamic random access memories, electromagnetic sensors or biomedical imaging and therapies¹⁻³.

In addition to the purely magnetic species, NPs of materials with both the intrinsic magnetization and electric polarization entered to the scene. The so-called multiferroic compounds with coexistence of at least two types of ferroic order (e.g. magnetic order and electric charge order) emerged as promising successors of the 'just' magnetic NPs. The benefit of such systems is the unambiguous coupling of magnetization to the other macroscopic property, like electric polarization. Consequently, the key ferroic parameters (typically direction of the magnetization and electric polarization) can be controlled by manifold external stimuli, e.g. using magnetic and electric field, mechanical deformation or light. The choice of intrinsic variables and possibility of their multiple control opens door to design of smart sensors and nanoelectronic devices based on multiferroics⁴⁻⁶.

In the family of the spinel oxides, multiferroic properties were reported for several spinel chromite phases. Among them the cobalt chromite is a very unusual multiferroic material with complex magnetic phase diagram. The cobalt chromite crystallizes in a cubic 'normal' spinel structure, $Fd\bar{3}m$, in which Cr^{3+} occupy the B sites (16d) and Co^{2+} the A sites (8a). On cooling the magnetic moments undergo a transition from paramagnetic to collinear ferrimagnetic state at $T_C \sim 93$ K, followed by additional order-to-order magnetic phase transition to incommensurate spiral (conical) spin structure at $T_S \sim 27$ K with propagation vector of the spiral component along the [110] direction. Finally, the ground state magnetic phase orders below the so-called lock-in temperature, $T_L \sim 14$ K. The ferroelectric order coincide with the T_S and the direction of the spontaneous polarization is fixed to [-110] for magnetization parallel to [001]; both unambiguously fixed to the propagation vector of the spiral component. (along [110]). It was also demonstrated that the spontaneous dielectric polarization and magnetization are of purely spin origin⁷⁻¹².

The character of magnetic order projected in the dielectric response is strongly dependent on the particle size, especially when approaching the critical coherence length of the spiral magnetic structure¹³⁻¹⁷ or varying the B-site occupation¹⁸. Alongside with the fascinating fundamental physical properties, the cobalt chromite phase, especially in sub-micron particles is demanded material and has been already utilized as inorganic pigment and efficient catalyst¹⁹⁻²². For that purpose, facile preparation of well-defined NPs of cobalt chromite is the key starting point for understanding spin-induced multiferroic properties when emerging critical particle size and consequently development of nanoscale devices with multiple addressing and controls.

Up to date, cobalt chromite NPs were prepared by sonochemistry²³, thermolysis²⁴, co-precipitation^{15;16;25}, sol-gel method^{26;27}, autocombustion^{28;29}, solvothermal *in situ* reduction³⁰ and variants of the hydrothermal method^{14;31;32}. In most of the above-described procedures, the as-prepared products were subjected to annealing at high temperatures in order to get nanocrystalline phase of the cobalt chromite. The final products thus consisted of cobalt chromite NPs in form of nanocrystalline powders. Moreover, the thermal post treatment often lead to aggregation or sintering, so the NPs were finally in direct contact. Consequently, such NPs are not ideal for studies of size-dependent magnetic properties as the direct contact may bring non-negligible changes of the surface spin structure and bring complications to the interpretation of magnetic measurements. Moreover, nanopowders are hardly re-dispersible in solvents, which prevent their further use for surface modification by ligand exchange usually carried out in liquid phase. The versatility of surface functionalization of the NPs is thus as a prerequisite for their incorporation in hybrid nanostructures and nanocomposites, for example using a versatile approach based on sol-gel method³³ or the click chemistry art³⁴⁻³⁶.

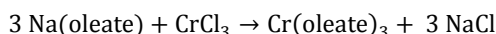
Here we present for the first time a facile preparation route yielding pure isolated cobalt chromite NPs without need of thermal post treatment procedure. In order to obtain the ternary spinel phase directly, the high temperature hydrothermal preparation (at reaction temperature about 250 °C) in water-alcohol-oleic acid system at high pressure was carried out. The route leads to uniform NPs capped with covalently bonded oleic acid, which prevents their direct contact and makes the NPs easily dispersible in non-polar solvents; thus suitable for various ligand exchange procedures. Our study is completed with detailed characterization of the NPs by powder x-ray diffraction, transmission electron microscopy, small-angle x-ray scattering, and vibrational spectroscopies. In addition, magnetic properties by means of temperature and magnetic field dependent magnetization and frequency-dependent a.c. susceptibility completed with polarized neutron scattering experiments down to low temperatures are also presented, and the impact of NP size on collapse of the long range magnetic ordering is discussed. Finally, perspectives of using the easily dispersible NPs of the multiferroic cobalt chromite are given.

2. Experimental section

Materials. The synthesis of cobalt chromite NPs was carried out using commercially available reagents: oleic acid (Sigma-Aldrich, tech. 90%), NaOH (Lach-ner, micropearls, p.a.), FeCl₃·6H₂O (Sigma-Aldrich, ≥98%), CoCl₂·6H₂O (Penta-chemicals, p.a.), ethanol (Lach-ner, absolute), hexane (Lach-ner 81.8%), distilled water. All chemicals were used as-received without further purification.

Synthesis of CoCr₂O₄ NPs. High temperature hydrothermal synthesis was proposed for the preparation of cobalt chromite NPs. First, a solution of sodium oleate was prepared from 10 mmol (0.40 g) of sodium hydroxide, which was dissolved in a small amount of ethanol and water mixture and adding 12 mmol (3.39 g) of oleic acid. A clear, homogeneous solution of sodium oleate was obtained. The water solution of oleate precursors was prepared from chromium and cobalt chlorides (molar ratio Cr³⁺ : Co²⁺ = 2:1). The reaction was carried out in total amount of 10 ml of water and 10 ml of ethanol. The water solutions of precursors and

sodium oleate were mixed together and put into ultrasonic bath for 5 min. After sonication, the reaction mixture formed two phases (water and organic), and the following reactions took place:



This resulting reaction mixture was put into the autoclave and placed in oven for 16 hours at the desired reaction temperature (the pressure inside autoclave reached 50 bar; all parameters of the preparation for the three samples are listed in Table 1). After cooling down the autoclave, the NPs were isolated from the crude solution by centrifugation in several dispersion/precipitation cycles using solvent - non-solvent pair (n-hexane/ethanol). Finally, the bluish-green dispersion of uniform cobalt chromite NPs capped with oleic acid in hexane was obtained.

Structural characterization. Powder x-ray Diffraction (PXRD) was performed using a PANalytical X'Pert PRO diffractometer with Cu K α radiation ($\lambda = 1.54 \text{ \AA}$) equipped with a secondary monochromator and PIXcel detector. All samples were measured in the 2θ range of $15 - 80^\circ$ with a step size of 0.02° . Calibration was done using the powder standard sample LaB $_6$ (SR 660b) purchased from NIST. The particle diameter by means of size of the coherently diffracting domain was determined by the Rietveld analysis using the Full Prof software³⁷. The instrumental broadening of the diffraction lines was also considered.

Morphological characterization. Transmission Electron Microscopy (TEM) was carried out using the LVTEM device operated at 5 kV with Schottky emitter (DeLong) and JEOL JEM 2200FS operated at 200 kV with Schottky emitter using bright field (BF) mode and electron diffraction (ED). The samples were obtained by dropping the dispersion on the coated copper grid. ED was performed at camera lengths of 40 cm or 60 cm.

Small-angle x-ray scattering (SAXS) measurements were carried out using the gallium anode low-angle x-ray instrument (GALAXI)³⁸ at JCNS, Forschungszentrum Jülich, equipped with a Pilatus 1M detector, parabolic optics and 4 m long collimation. For the SAXS measurement, dispersions of NPs were filled in glass capillaries. An x-ray wavelength of $\lambda = 1.34 \text{ \AA}$ and detector distances of 853 and 3548 mm were used for the measurement. The data were collected using a two-dimensional (2D) detector and corrected for contributions of the cell with solvent, thickness and transmission. The scattered intensity was calibrated to absolute units using a FEP 1400A ($d = 0.35 \text{ mm}$) standard measurement. The SAXS data were fitted using Beaucage model with two levels, which characterizes the Guinier and Porod regions with smooth transition between them and yields a radius of gyration and Porod exponent.

Elemental analysis. Thermogravimetric analysis (TGA) was carried out using the device of Setaram. The samples were heated up to $600 \text{ }^\circ\text{C}$ (heating rate $10 \text{ }^\circ\text{C}/\text{min}$) in argon atmosphere with nitrogen $40 \text{ ml}/\text{min}$. A complementary energy dispersive analysis was also performed on the Tescan Mira I LMH device with the energy dispersive x-ray detector (EDX) Bruker AXS. The NP powders were deposited on carbon film to diminish charging during the experiment.

Vibrational spectroscopies. Fourier transform infrared (FTIR) spectra were obtained using Thermo Scientific Nicolet 6700 FTIR Spectrometer (resolution 2 cm^{-1} , DTGS detector, KBr beamsplitter, Happ-Ganzel apodization, KBr windows) in the region $400 - 4000\text{ cm}^{-1}$ with diffuse reflectance infrared Fourier transform spectroscopy (DRIFTS) technique. The nanocrystalline samples were mixed with KBr (for IR spectroscopy, Merck). Raman spectra of nanocrystalline samples were measured using Thermo Scientific DXR Raman Microscope with Olympus microscope (objective 50x) in the spectral range of $50\text{-}1900\text{ cm}^{-1}$ with a resolution of 3 cm^{-1} . He-Ne laser or diode lasers (532 and 780 nm) were used for the measurement. The spectrometer was calibrated using multiple neon emission lines and multiple polystyrene Raman bands and standardised by white light.

Magnetization and a.c. susceptibility. The temperature dependence of the zero-field-cooled (ZFC) and field-cooled (FC) magnetization and the magnetization isotherms at selected temperatures were measured using the Quantum Design MPMS7XL device (SQUID magnetometer). The ZFC-FC measurements were carried out between 2 and 300 K with 2 K/min sweep in the applied magnetic field of $\mu_0 H = 10\text{ mT}$, after cooling in either applied (FC) or in zero field (ZFC). Temperature dependent a.c. susceptibility was recorded in zero external magnetic field at frequencies of $f = 0.1, 1, 10, 10^2$ and 10^3 Hz with an a.c. magnetic field amplitude of 0.3 mT . The powder samples with mass about 5 mg were put into gelatine capsules and fixed with a piece of polystyrene during the experiments. The magnetization values were corrected to the content of the oleic acid.

Polarized neutron scattering. Polarized neutron scattering with XYZ polarization analysis was carried out at the Diffuse Neutron Scattering (DNS)³⁹ instrument at Heinz Maier-Leibnitz Zentrum. The six polarized scattering contributions by cobalt chromite nanoparticles as well as $\text{Ni}_{0.89}\text{Cr}_{0.11}$ standard and vanadium references were measured in a wide scattering momentum range of $0.5 < Q < 3.4\text{ \AA}^{-1}$. The measurements were carried out at aluminium sample holder using a temperature of 4 K and 100 K and a neutron wavelength of $\lambda = 3.3\text{ \AA}$. The magnetic, nuclear and nuclear spin-incoherent scattering contributions were separated from the total scattering cross section by means of XYZ- polarization analysis in the spin flip (SF) and non-spin flip (NSF) channels. Separation of the observed data was performed using DNS polarization analysis algorithm. The reference measurement of a $\text{Ni}_{0.89}\text{Cr}_{0.11}$ alloy yields the flipping ratio correction and thus the real polarization of the incident neutron beam. Background correction is performed by measurement of the empty aluminium sample holder and subtraction from the raw data. Vanadium was measured for calibration of the detector efficiency.

3. Results and Discussion

3.1. Synthesis of nanoparticles

Cobalt chromite NPs with covalently bonded oleic acid were successfully synthesized by hydrothermal decomposition of cobalt(II) and chromium(III) oleates in water-ethanol system. The reaction temperature was adjusted above the range (180 to $200\text{ }^\circ\text{C}$) common for preparation of ferrite NPs⁴⁰⁻⁴² due to the higher decomposition temperature of the chromium (III) oleate in comparison to the iron(II), (III) and cobalt(II)

oleates. This hypothesis was tested on two preparation protocols applied to the cobalt ferrite NPs as a reference. First the general route in water-alcohol-fatty acid system introduced by Wang and co-workers⁴⁰ was carried out using the same parameters of the reaction (reaction temperature: 180 - 200 °C, amount of oleic acid and solvents, ratio of metal oleates). In this general route the NPs are formed from the *in situ* generated metal oleates. Using this preparation route, cobalt ferrite NPs with size up to 8 nm were obtained⁴¹, while successful preparation of the cobalt chromite NPs was not possible without additional annealing¹⁴. The same result was obtained when using the hydrothermal decomposition of *ex situ* prepared metal oleates at the maximum temperature of 200 °C. While decomposition of the cobalt (II) oleate in high pressure autoclave occurs at around 170 °C and cobalt ferrite NPs can be easily prepared⁴², the chromium (III) oleate decomposes at higher temperature (240 °C); thus only amorphous residuum is obtained. For this reason the reaction temperature was adjusted close to the decomposition temperature of the chromium (III) oleate. The updated procedure leads directly to the NPs of the desired spinel phase coated with oleic acid. Consequently, the NPs can be easily dispersed in hexane. The greenish dispersion of the cobalt chromite NPs in various non-polar solvents was found to be stable against precipitation for months. Moreover, the size of the NPs can be tuned up to some extent by varying the reaction temperature as with the increase of the reaction temperature, the size of the NPs also increases.

3.2. Morphological and structural characterization

First, the morphology of the cobalt chromite NPs was characterized using the TEM and SAXS. Typical TEM micrographs presented in Figure 1 (top) reveal nearly spherical shape of the NPs with the mean particle diameter of 3.0(1), 3.2(1) and 4.2(1) nm and log normal size distribution of 13.0(2), 12.0(1) and 16.1(1) % for S₁, S₂ and S₃ sample, respectively (for details, please see the Supplementary material).

The results of the SAXS experiment together with the fit of the experimental data are shown in Figure 1 (bottom). The fitted value of the fractal dimension lies between 1 and 2. According to the study of Bonini⁴³ the Porod exponent equal to 1 suggests formation of chain-like aggregates. In our case the Porod exponent is close to 1.5, which suggests formation of branched assemblies of the NPs. Such structures were also observed in the TEM micrographs (Figure 1a marked with orange squares) and they are typical for NPs prepared by the variants of the hydrothermal route in water-alcohol-fatty acid system^{40;41}. At higher Q range the Q^{-4} asymptotic behaviour was observed, which corroborates the spherical shape of the NPs observed by the TEM. The obtained spherical radius, R_s is related to the gyration radius, R_G according to $R_s = (5/3)^{1/2} \cdot R_G$. The spherical radii determined from the SAXS data (Table 2) are in good agreement with those obtained by the TEM analysis. A second parameter, which can be obtained at lower Q range corresponds to the size of potential aggregates. The average size of the aggregates is given in Table 2. The tendency to aggregation of the dried NPs was also observed in the TEM (Figure 1a marked with orange rectangle).

The phase analysis was carried out using powder x-ray and electron diffraction, respectively. Both experiments confirmed the presence of the cobalt chromite spinel structure in the NPs (Figure 2a and Figure 2b) with the space group $Fd\bar{3}m$ (card No. JCPDF 22- 1084). The values of the refined lattice parameter a and the particle size (diameter, d_{PXRD}) are summarized in Table 3 and Table 2, respectively. Both values increase

with increasing reaction temperature for all prepared samples as expected. The $d_{\text{PXR D}}$ value is somewhat smaller in comparison to the size derived from the TEM and SAXS. This fact is in good agreement with the general expectation that the particle size derived from the PXRD is related to the coherently diffracting domain size, which is usually smaller than the physical size of the whole particle, even for highly crystalline NPs. The $\text{Co}^{2+} : \text{Cr}^{3+}$ ratio was determined using EDX analysis and the values close to the nominal 1 : 2 stoichiometry were found for all samples.

View Article Online
DOI: 10.1039/C6RA21377D

The content of the oleic acid in the prepared NPs was evaluated using the TGA analysis (Figure 3a). During the TGA, the decomposition of the prepared samples occurs in two steps. The first step represents the process of dehydration of samples up to 220 °C. The second step corresponds to the decomposition of the oleic acid on the surface of the NPs.

The covalent nature of the bond of the oleic acid to the NPs was then confirmed by the FTIR spectroscopy; the spectra are shown in the Figure 3b and all assignments are summarized in Table 4. The Raman spectra of the chromite NPs were also measured as a complementary probe of the vibrational states in the spinel chromite phase. They are shown in Figure 3c for the S₁ and S₃ samples. All Raman active bands (A_{1g} , F_{2g} , E_g) were assigned according to the theoretical vibrational representation $t_2g + t_2g + e_g$. The explicit positions of the Raman bands were detected as follows: 674, 635, 592, 575, 509, 454 and 191 cm^{-1} and 671, 634, 589, 578, 523, 507, 461, 447 and 190 cm^{-1} for the S₁ and S₃ sample, respectively. In comparison to the bulk sample of the cobalt chromite⁴⁴ the Raman bands of the NPs show a predominant shift towards lower wavenumbers. However, the values are close to those of the nanosized cobalt chromite particles reported by other authors³². The overall downshift of the Raman bands can be well understood in terms of the size effect as in oxide materials the size reduction results in the increase of the micro-strain and/or dominance of the phonon confinement⁴⁵.

3.3. Magnetic properties

Magnetic properties of the S₁ - S₃ samples were finally investigated and interpreted in context of previous studies on NPs prepared by other routes with larger particle size. In order to compare the magnetic behaviour of the NPs to the bulk material, the temperature dependencies of the magnetization recorded in moderate external magnetic field of 10 mT in zero-field cooled (ZFC) and field-cooled (FC) regimes were carried out. The resulting curves are presented in Figure 4a. The ZFC curves show a clear single maximum for all samples at a temperature termed T_{max} (the values for all samples are listed in the Table 5). In addition, a bifurcation point of the ZFC and FC curves was observed at slightly higher temperature. The values of the T_{max} are depicted in Figure 4b in comparison to the values obtained for larger NPs prepared by the same route, but subjected to additional heat treatment, and the T_c of the bulk cobalt chromite. The T_{max} values are almost identical for all samples and fall to the monotonous dependence on the particle size. However, the rapid degrees with respect to the decreasing particle size suggests change of the intrinsic magnetic structure in the NPs. The hypothesis is corroborated by the character of the first order derivatives of the ZFC and FC curves, shown in Figure 4c. In the bulk sample the sharp minimum of the ZFC curve below the T_c is expected¹³, while there is a rather broad minimum of the ZFC curve for all investigated samples, which is

usually related to the disorder effects in NPs and subsequent reform of the exchange interactions due to the disorder⁴⁴. In extreme case, the collapse of the bulk-like magnetic order can be observed, which is characterized by the onset of short-range order or glassy like spin state⁴⁶. Moreover no additional sharp extreme in the ZFC curve and the related $M(T)$ derivatives was observed; thus the order-to-order magnetic phase transitions observed at the T_s and T_L in the bulk cobalt chromite are not evidenced in the NPs. As reported previously, the disorder effects are significant for cobalt chromite NPs with crystallite size 4 - 6 nm¹⁴; thus they are expected to dominate the magnetic response of the NPs with crystalline size below 4 nm as is the case of the S₁ - S₃ samples.

The temperature dependencies of the ZFC-FC magnetization were completed by measurements of magnetization isotherms for all prepared samples in the temperature range 2 K - 100 K in the magnetic field up to ± 7 T. The obtained $M(H)$ curves are shown in Figure 5a. A considerable hysteresis opens below the T_{max} reaching the coercivity, $\mu_0 H_c$ about 0.6 T and 0.8 T at 2 K for the S₂ and S₃ samples, respectively. The hysteresis loop of the S₁ sample recorded at 2 K is constricted yielding $\mu_0 H_c \sim 0.1$ T. A similar deformation of the hysteresis loops is usually attributed to the coexistence of at least two magnetic phases with very different coercivities (soft and hard magnetic phase)⁴⁸. As the phase analysis unambiguously confirmed single phase nature of the sample, the constriction of the loop is rather originated by different types of the spin order coexisting within a single NP. This explanation is corroborated by the study of exchange bias in ~ 5 nm large cobalt chromite NPs, where the frozen and rotatable spins coexist in a single NP due to the size driven spin disorder⁴⁷. The complexity of spin texture in the S₁ sample is also coherent with the relative fraction of disordered spinel structure in comparison to the S₂ and S₃ samples as the spin disorder is closely related to the crystallographic disorder. The value can be estimated by comparison of the volumes of the coherently diffracting domain (crystalline part) to the physical volume derived from the TEM. Therefore in the S₁ sample with about 40 % of the volume disorder, the deviation of the spin structure and its complexity is more favoured than in the S₂ and S₃ samples with the structural disorder about 30 % of the whole volume.

The complexity of the spin structure is also mirrored in the size dependence of the coercivity determined below the T_{max} shown for all samples in Figure 5b. The S₂ and S₃ $\mu_0 H_c$ values are more than one order of magnitude higher than the coercive field reported for a bulk single crystal⁴⁶ (0.1 T), however; there is no clear correlation of the $\mu_0 H_c$ values with the particle size (determined by the PXRD, TEM and SAXS). The constriction of the loop of the S₁ sample also prevents any simple size correlation. However; similar observations were reported by Zhu and co-workers for nanopowders of cobalt chromite prepared by hydrothermal decomposition of metal hydroxides⁴⁸. Finally, the hysteresis loops show no trend to saturation up to 7 T, likely due to formation of a glassy-like state associated with the overall spin disorder due to the very low particle size^{14;49}. Above the T_{max} , the hysteresis disappears and the magnetization follows the Brillouin-like dependence as expected for paramagnetic state. For completeness, the values of the spontaneous magnetization below the T_{max} are depicted in Figure 5c. They clearly decrease on heating due to increasing spin fluctuations resulting in decrease of the average magnetization values.

The questionable nature of the magnetic state below the T_{max} was finally inspected by polarized neutron scattering experiments carried out on the S₂ sample. No additional diffraction peaks, which could be

associated with long range magnetic order were detected alongside with the diffractions identified in the paramagnetic state (see Figure 2S in Supplementary Information file). Therefore any speculations on persistence of long-range magnetic order in the spinel chromite NPs with size below 4 nm can be unambiguously excluded. Thus the anomaly observed on the ZFC - FC dependencies can be attributed to the glassy state formed due to collapse of the long-range magnetic order as the particle size is lower than the characteristic coherence length of the spiral component in the ground state magnetic structure⁴⁶. Our results also exclude hypothesis on formation of the superparamagnetic (SPM) state for such small particles of cobalt chromite, which has similar fingerprints on the ZFC-FC curves. The SPM state requires formation of a single-domain state, which is possible only for materials with long-range ferromagnetic or ferrimagnetic order.

The dynamic spin properties of the glassy state were further investigated by measurements of the real (χ') and imaginary (χ'') parts of the a.c. susceptibility with varying frequency (f) of the alternating magnetic field with the amplitude of 3 mT; the results for the real (χ') component are shown in Figure 6. The temperature dependence of the χ' reveals a shift of the characteristic maximum, T_m with increasing f . This phenomenon is deemed as a consequence of the spin relaxation. The spin dynamics was first inspected by evaluating a phenomenological parameter ϕ , which represents a shift of the T_m (ΔT_m) per frequency decade:

$$\phi = \frac{\Delta T_m}{T_m \cdot \Delta \log f},$$

where the ΔT_m represents shift of the maxima on the real part of a.c. susceptibility and f is the actual frequency. The corresponding ϕ values are: 0.04(1), 0.03(1) and 0.03(1) for the S₁, S₂ and S₃ sample, respectively. The ϕ values falling in the interval of 0.02 - 0.05 typically suggest formation of concentrated spin glass or cluster-glass states, dominating usually the response of the surface layers of the NPs^{50;51}.

As suggested by the static magnetic experiments, significant disorder resulting in collapse of magnetic order and onset of spin-glass like state is expected. Thus, the a.c. susceptibility data were subjected to analysis by the Vogel-Fulcher law⁵²:

$$\tau = \tau_0 \cdot \exp\left(-\frac{K_{\text{eff}}V}{k_B(T-T_{\text{VF}})}\right),$$

where τ_0 is the characteristic relaxation time of the individual spins, V is the volume of NP, K_{eff} is the effective anisotropy constant and T_{VF} is the Vogel-Fulcher temperature, which is often attributed to the strength of particle interactions, but has no real physical meaning. Finally, the critical spin dynamics was also inspected using the power law⁵³ in the following form:

$$\tau = \tau_0 \cdot \left(\frac{T_m}{T_g} - 1\right)^{zv},$$

where τ_0 is the characteristic relaxation time, T_g represents the temperature of transition to the glassy state and zv is the critical power exponent. The best fits to the experimental data using both approaches are shown in Figure 7 and the resulting values are listed in Table 6. The τ values are of few orders of magnitude larger than usually reported for canonical spin glasses ($\tau \sim 10^{-12}$ s), but comparable to the values reported for

substituted spinel phases with short-range ferrimagnetic ordering^{13,48}. Thus strong correlation between the constituent spin units suggests condensation of the collective cluster glass like state in our spinel chromite NPs.

4. Conclusions

High temperature hydrothermal synthesis without need of additional thermal treatment has been developed to produce uniform cobalt chromite NPs with size distribution of 12 – 16%. The optimized route leads to the formation of cobalt chromite NPs capped with covalently bonded oleic acid with mean particles diameter in the range of 3.0(1) – 4.2(1) nm. Thanks to the hydrophobic coating, the NPs can be easily dispersed in non-polar solvents; the dispersion was found to be stable over months. The formation of pure spinel cobalt chromite phase was observed by x-ray and electron diffraction. The FTIR measurements confirmed the presence of covalently bonded oleic acid, which causes their hydrophobic properties. The uniform spherical shape of the NPs was confirmed by the TEM and SAXS experiments. The characteristic fractal dimensions obtained from the SAXS point to the formation of branched structures.. The investigation of the magnetic properties suggested strongly reformed behaviour in comparison to the bulk material due to the very low particle size. Magnetic phase transitions reported for the bulk cobalt chromite were not observed in the NPs; instead the glassy like state emerges with the transition temperature in the interval of 11.6(1) – 14.5(1) K. The collapse of long-range magnetic order was unambiguously confirmed by the neutron scattering experiments. The spin dynamics of the glassy-like state studied by the a.c. susceptibility revealed values of the spin relaxation time typical for collective spin glass behaviour with short-range correlations between the disordered spins, located dominantly in the surface proximity. The successful preparation of the uniform NPs of the cobalt chromite as the archetype multiferroic phase is the important key to understand the mechanism of coupling between the magnetization and polarization when approaching critical NP size, where the magnetic long range order collapses. Moreover, availability of dispersible cobalt chromite NPs opens door to numerous preparation strategies aiming to incorporation of the multiferroic NPs in smart hybrid nanostructures and nanocomposites using general concepts such as the sol-gel chemistry or the click chemistry art, which both require possibility of custom functionalization of the NPs in liquid phase as the kick off point.

Author information

View Article Online
DOI: 10.1039/C6RA21377D

Corresponding Authors

*zakutna@ill.fr, vejpravo@fzu.cz

Present Addresses

†Department Chemie, Universität zu Köln, Luxemburger Strasse 116, 50939 Köln, Germany. Institut Laue-Langevin, F-38042 Grenoble, France.

Author Contributions

‡These authors contributed equally.

Acknowledgments

This work was supported by the Long-Term Research Plan of the Ministry of Education of the Czech Republic (MSM0021620857) and Czech Science Foundation (project no. 15-01953S). Magnetic measurements were performed in MLTL (see: <http://mltl.eu>), which is supported within the program of Czech Research Infrastructures (project no. LM2011025). We acknowledge JCNS for providing of neutron scattering facility at DNS instrument. The presented work was financially supported by the Ministry of Education, Youth and Sport Czech Republic Project LQ1603 (Research for SUSEN). The results were partially developed within the CENTEM project CZ.1.05/2.1.00/03.0088 through CENTEM PLUS (LO1402) from the Ministry of Education, Youth and Sports under the National Sustainability Programme I.

Abbreviations

NPs, nanoparticles; PXRD, powder x-ray diffraction; TEM, transmission electron microscopy; SAXS, small-angle x-ray scattering; ED, Electron Diffraction; EDS, energy disperse spectroscopy; FTIR, Fourier transform infrared; DRIFTS, diffusion reflectance infrared Fourier transform spectroscopy; ZFC, zero-field cooled; FC, field cooled; SQUID, superconducting quantum interference device; DNS, diffuse neutron scattering; SF, spin flip; NSF, non-spin flip.

Figures

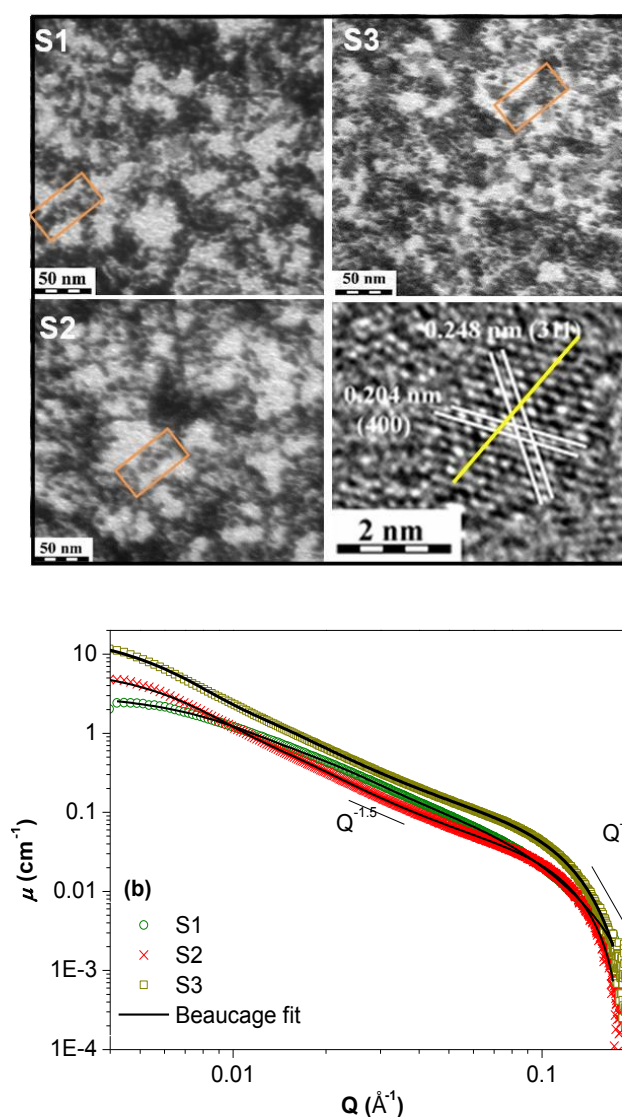
View Article Online
DOI: 10.1039/C6RA21377D

Figure 1 (Top) Bright field TEM micrographs of the S₁ - S₃ samples. The orange marks indicate chain-like aggregates. The last image shows the HRTEM micrograph of S₁ sample with the diffraction fringes of (311) and (400) planes. The yellow line corresponds to the projected particle diameter. **(Bottom)** The results of the SAXS measurements of the S₁, S₂ and S₃ samples with Beaucage fits of the Porod exponents.

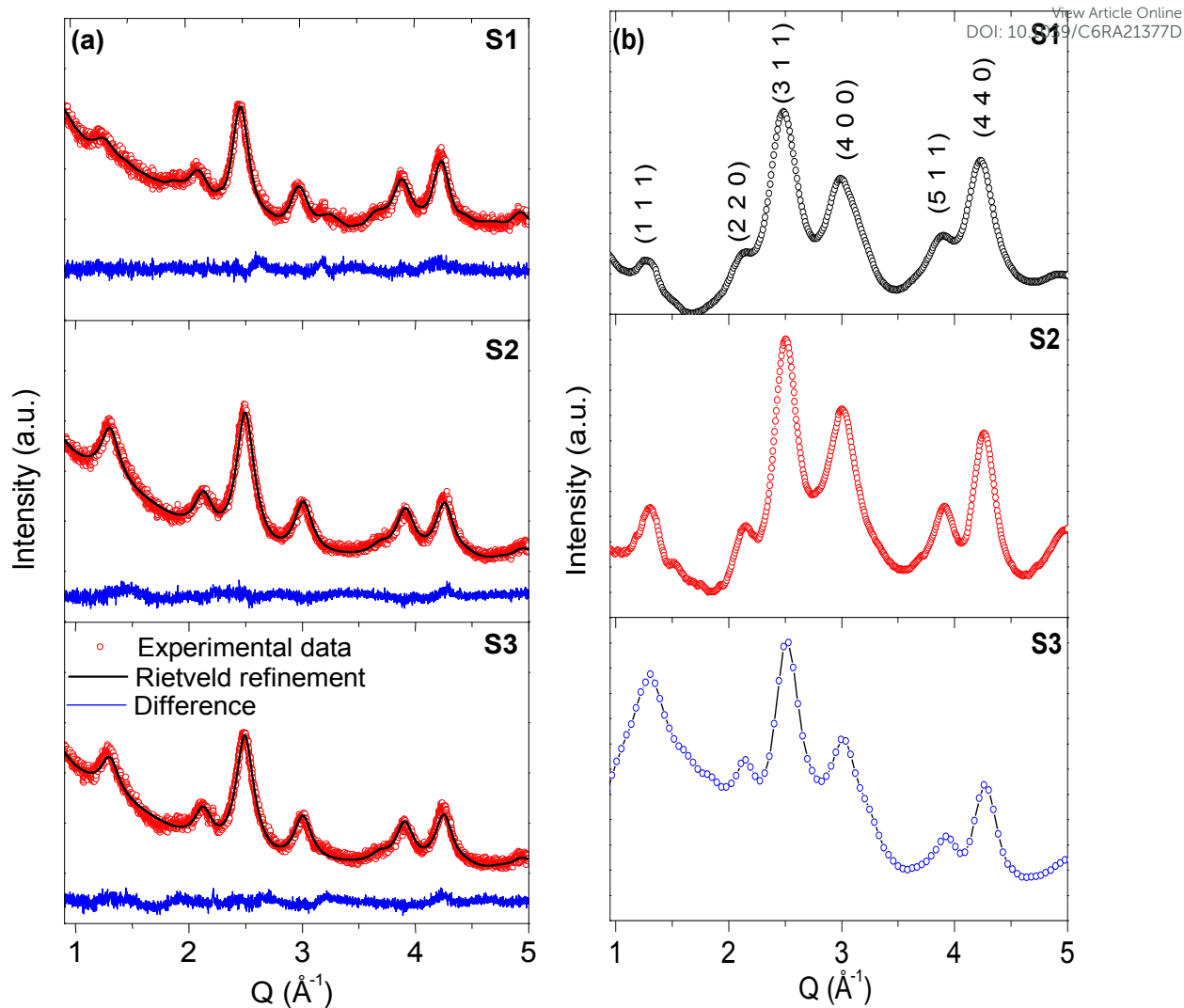


Figure 2 (a) PXRD data and their Rietveld refinement for the S₁ - S₃ samples. Observed, calculated and difference intensities are shown, in red, black and blue, respectively. (b) Results of electron diffraction (selected area) for the S₁ - S₃ samples.

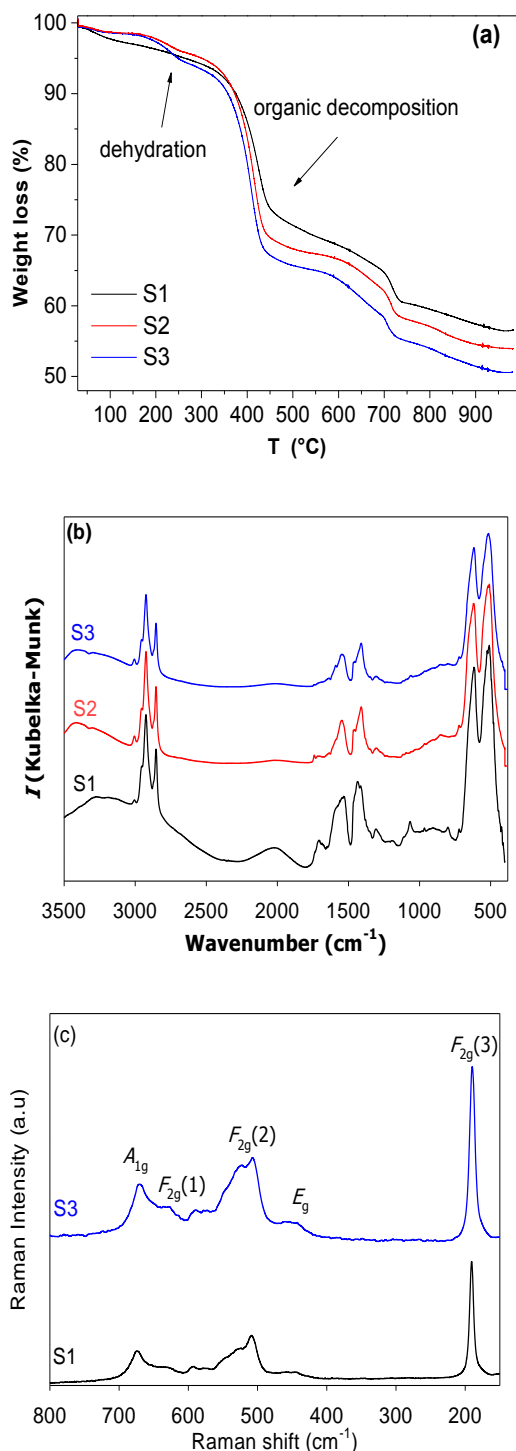


Figure 3 (a) Thermogravimetric curve of the S₁ - S₃ samples. (b) FTIR spectra of the prepared NPs coated by oleic acid (S₁ - S₃ samples) and (c) Raman spectra of S₁ and S₃ samples with assigned symmetry types of the Raman active bands.

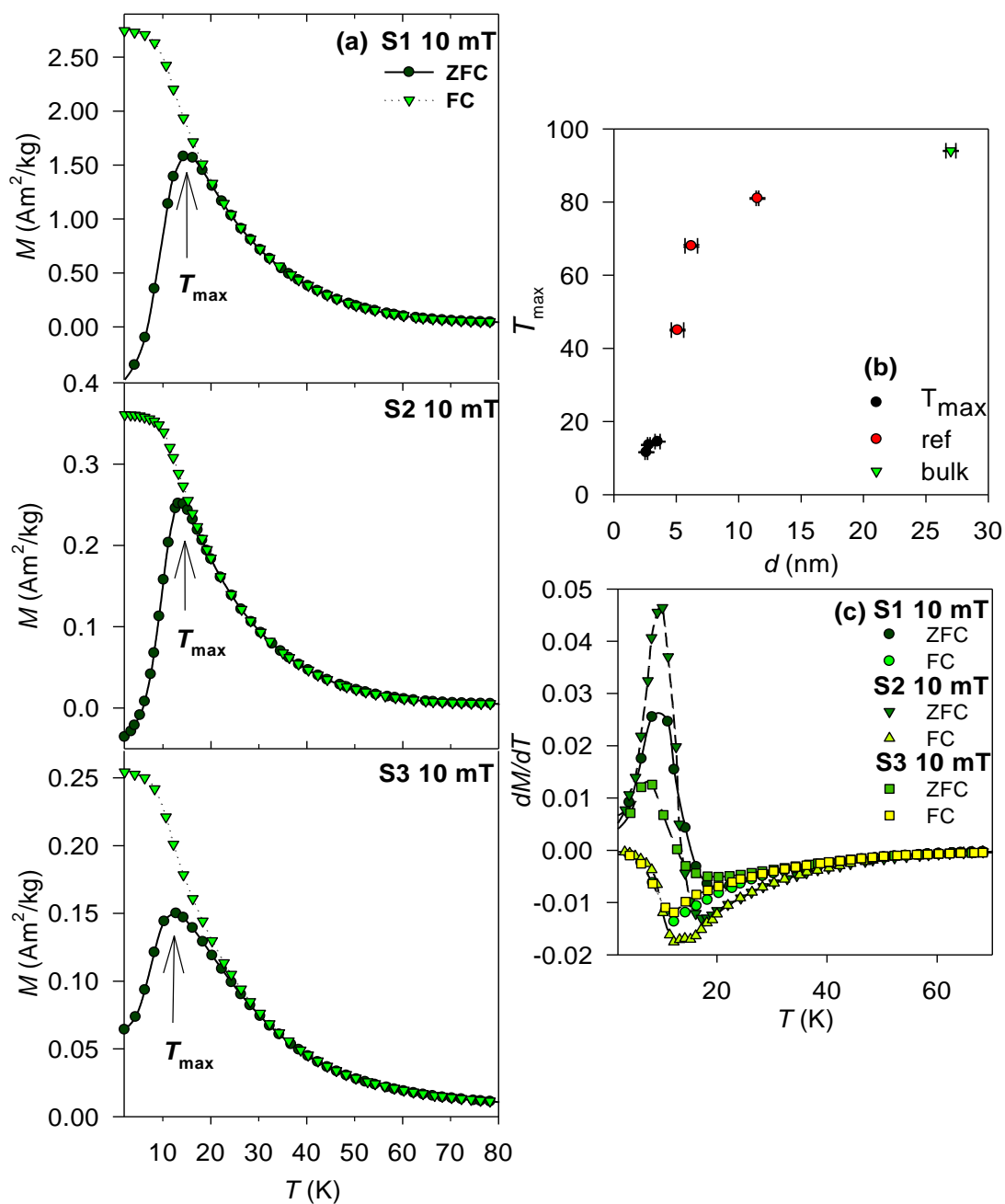


Figure 4 (a) ZFC-FC curves of the S₁ - S₃ samples recorded at 10 mT. (b) Size dependence of the T_{max} in comparison to the bulk and previously reported values¹⁴. (c) First derivatives of the ZFC-FC curves for S₁ - S₃ samples.

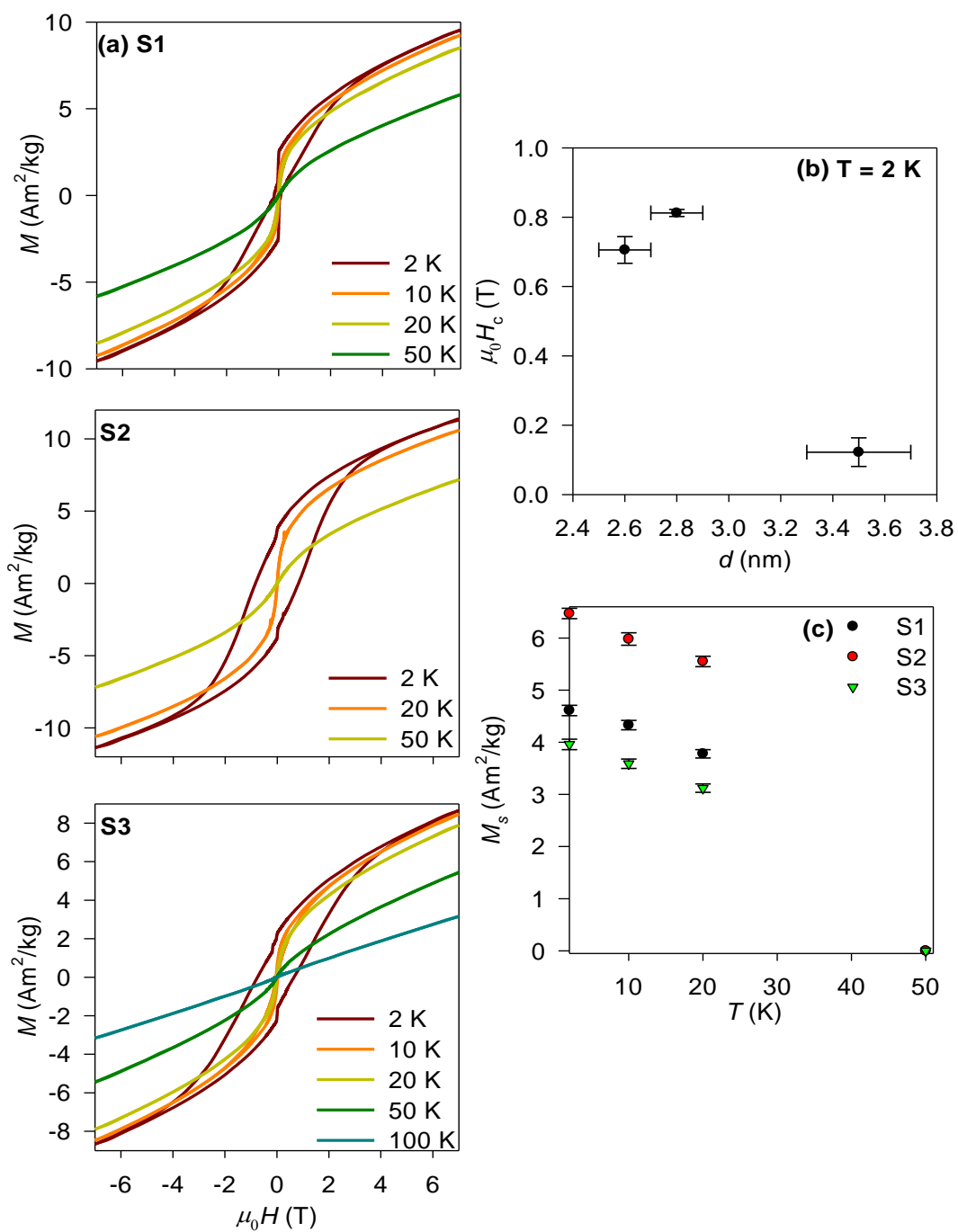


Figure 5 Magnetic properties of S₁ - S₃ samples. (a) Hysteresis loops at selected temperatures. (b) Dependence of the coercive field, $\mu_0 H_c$ at 2 K on particle size derived from PXRD. (c) Temperature dependence of spontaneous magnetization, M_s .

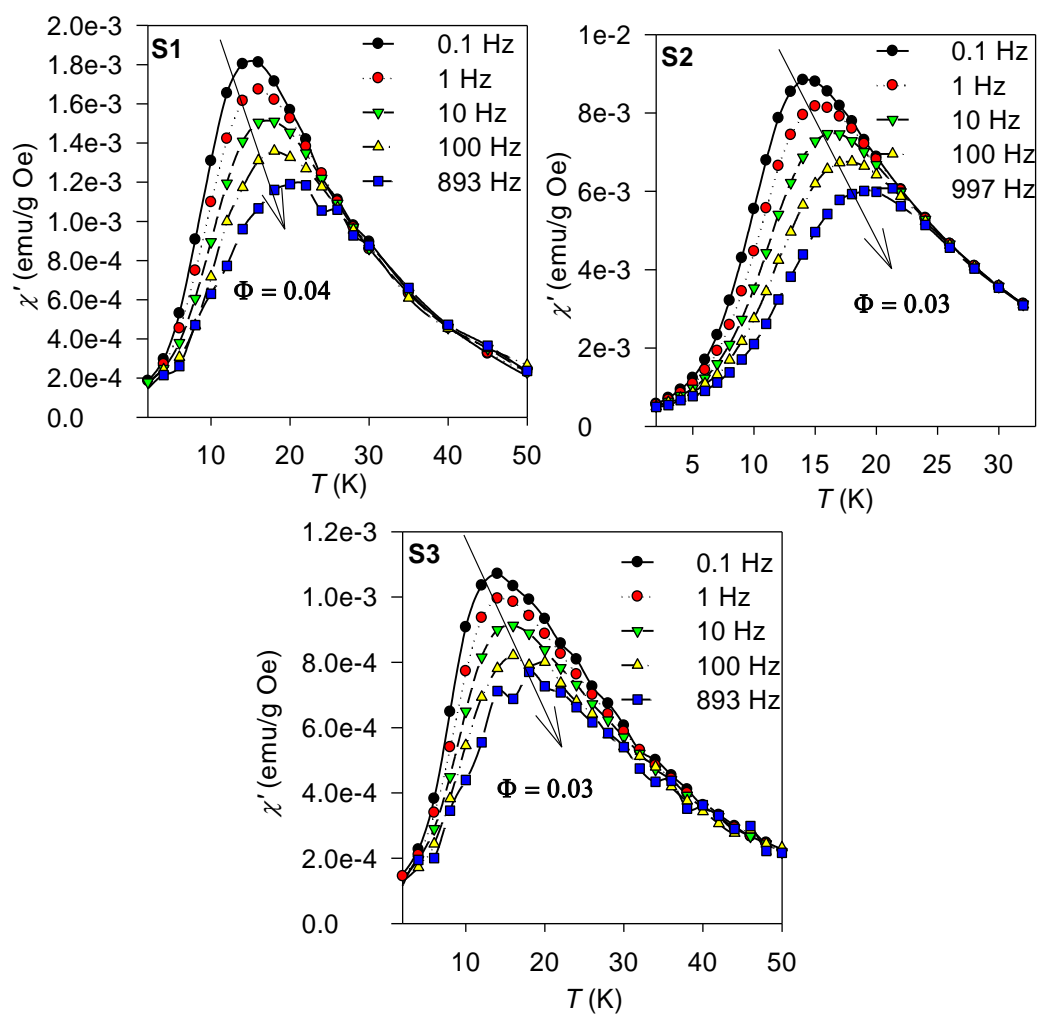


Figure 6 Real part of the a.c. susceptibility, χ' of the S1 - S3 samples measured at various frequencies.

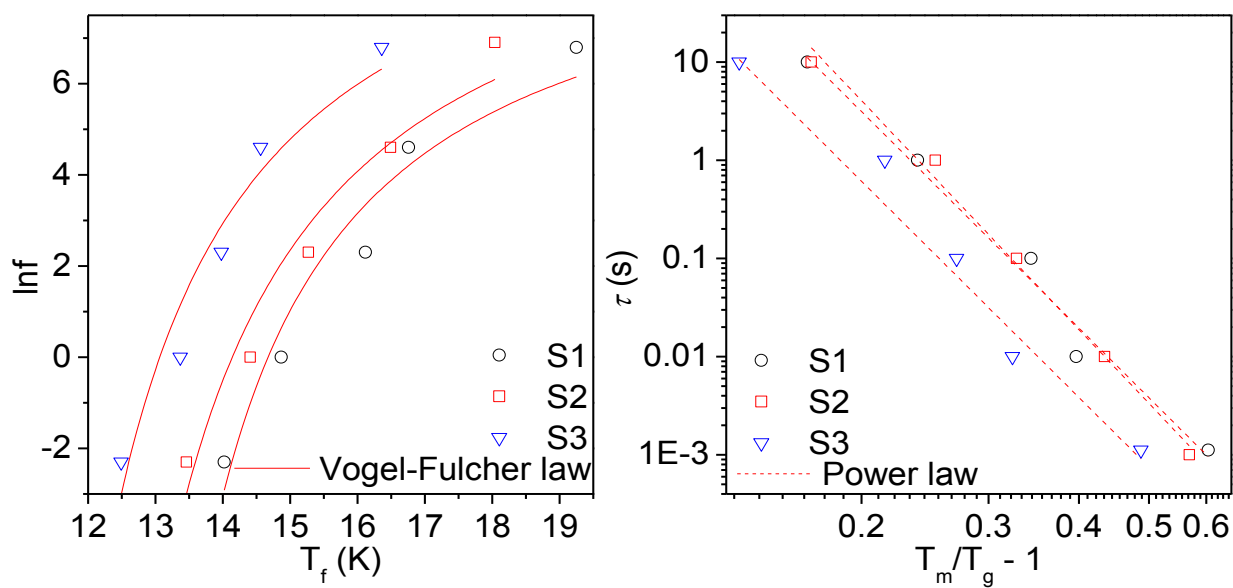


Figure 7 Vogel-Fulcher (left) and Power law (right) fits for S1 - S3 samples.

Tables

View Article Online
DOI: 10.1039/C6RA21377D

Table 1 Reaction conditions of the hydrothermal decomposition.

Sample	Temperature (°C)	Time (h)	Pressure in autoclave (bar)
S1	247	16	54
S2	240	16	47
S3	237	16	40

Table 2 The particle (or aggregate) size by means of diameter of the S₁ - S₃ samples obtained by various approaches^a.

sample	Particle size (nm)			Aggregate size (nm)
	d_{PXRD}	d_{TEM1}	d_{SAXS1}	d_{SAXS2}
S ₁	3.5(2)	4.2(1)	5.7(1)	49.1(1)
S ₂	2.8(1)	3.2(1)	4.4(5)	72.3(2)
S ₃	2.6(1)	3.0(1)	4.6(1)	82.6(1)

^a d_{PXRD} is size obtained from Rietveld analysis, d_{TEM1} is a mean size from log-normal distribution of size from TEM and d_{SAXS} ($d_{\text{SAXS}} = 2 \cdot R_g$) from Beaucage fits of SAXS.

Table 3 Results of the Rietveld analysis^b.

Refined parameter	Refined value		
	S ₁	S ₂	S ₃
a (Å)	8.374(1)	8.358(1)	8.337(1)
u	0.2563(1)	0.2652(2)	0.2567(1)
BOV (Å ²)	0.86(5)	2.1(1)	1.9(2)
Profile function	pseudo-Voigt function		
Y (°)	0.12(2)	1.16(1)	0.01(1)
GausSize (°)	3.76(4)	3.07(3)	4.65(3)
Background function	Chebyshev polynomial (13 refined parameters)		
zero (0.01°)	0.4(1)	0.2(1)	0.3(1)
R_B (%)	14.6	11.7	16.8
R_{wp} (%)	2.56	3.65	3.99
R_{exp} (%)	2.55	2.98	3.63
χ²	1	1.4	1.1

^bSymbol meaning: lattice parameter, *a*, position of oxygen atoms, *u*, an overall isotropic displacement, *BOV*, isotropic particle size broadening contribution, *Y*, an isotropic Gaussian size parameter, *GausSize*, zero position and Rietveld agreement factors.

Table 4 Assignment of the FTIR spectra for the S₁ - S₃ samples.View Article Online
DOI: 10.1039/C6RA21377D

Wavenumber (cm ⁻¹)			Assignment
S1	S2	S3	
	510 vs	510 vs	δ C-C
514 vs	518 vs		F _{1u} (2), δ OCO, δ CCO, δ CC
618 vs	618 vs	618 vs	F _{1u} (1), δ OCO, δ CCO, δ CC
722 w	722 w	721 w	ρ CH ₂
1062 w		1066 w	ν _{as} -C-C=C-
1306 wb	1305 wb	1307 wb	ν C-O + δ COH
1410 sb	1410 sb	1414 s	δ -CH ₂ CO-, ν C-O + δ COH
		1437 sb	ν C-O + δ OH
1456 sh	1456 sh		δ -(CH ₂) _n -
1548 sb	1548 sb	1534 sb	ν _s COO ⁻
1706 mb	1741 mb	1707 mb	ν C=O
2854 s	2853 s	2853 s	ν -CH ₂ -
2924 s	2924 s	2924 s	ν -CH ₂ -
2955 s	2955 s		ν -CH ₃ , ν -CH ₂ -
3006 mb	3006 mb	3005 mb	ν -CH ₃
3300 mb		3273 mb	ν OH
3406 mb	3420 mb		ν OH

Table 5 Parameters (remanence, Mr coercivity, μ₀H_c and magnetization at 7T@2K, M_{s,2K}) obtained from the magnetization isotherms recorded at 2 K and maxima of ZFC, T_{max} obtained from magnetization temperature dependent measurements.

Sample	M _r (A·m ² ·kg ⁻¹)	μ ₀ ·H _c (T)	M _{s,2K} (A·m ² ·kg ⁻¹)	T _{max} (K)
S ₁	2.6±0.3	0.10±0.01	4.6±0.3	14.5±0.2
S ₂	3.8±0.4	0.80±0.08	6.5±0.4	13.6±0.1
S ₃	2.0±0.2	0.70±0.07	4.0±0.2	11.6±0.1

Table 6 Results from Vogel-Fulcher law and Power law^c.

Sample	Vogel-Fulcher law		Power law		
	τ (s)	T_{VF} (K)	T_g (K)	zv	τ (s)
S ₁	$(4.4 \pm 0.4) \cdot 10^{-5}$	12 \pm 2	12 \pm 2	7.3 \pm 0.5	$(2.4 \pm 0.4) \cdot 10^{-5}$
S ₂	$(1.5 \pm 0.2) \cdot 10^{-5}$	11 \pm 2	11.5 \pm 2	7.8 \pm 0.5	$(4.4 \pm 0.4) \cdot 10^{-5}$
S ₃	$(8.4 \pm 0.8) \cdot 10^{-6}$	10 \pm 2	11 \pm 2	7.3 \pm 0.5	$(4.7 \pm 0.5) \cdot 10^{-5}$

^cWhere τ is the attempt frequency, T_{VF} is Vogel-Fulcher temperature, T_g is glassy transition temperature and zv represents the power law exponent.

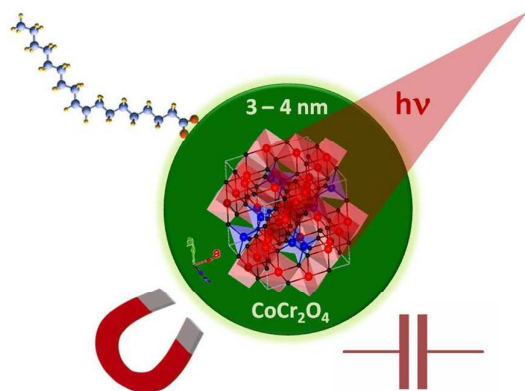
References

View Article Online
DOI: 10.1039/C6RA21377D

1. I. Hilger and W. A. Kaiser, *Nanomedicine*, 2012, **7**, 1443.
2. M. E. McHenry and D. E. Laughlin, *Acta Materialia*, 2000, **48**, 223.
3. Q. A. Pankhurst, J. Connolly, S. K. Jones, and J. Dobson, *Journal of Physics D-Applied Physics*, 2003, **36**, R167.
4. J. M. Hu, L. Q. Chen, and C. W. Nan, *Advanced Materials*, 2016, **28**, 15.
5. A. Aqeel, N. Vlietstra, J. Heuver, G. Bauer, B. Noheda, B. van Wees, and T. Palstra, *Physical Review B*, 2015, **92**, 224410.
6. R. Ramesh and N. A. Spaldin, *Nature Materials*, 2007, **6**, 21.
7. V. Tsurkan, S. Zherlitsyn, S. Yasin, V. Felea, Y. Skourski, J. Deisenhofer, H. von Nidda, J. Wosnitza, and A. Loidl, *Physical Review Letters*, 2013, **110**, 115502.
8. L. Chang, D. Huang, W. H. Li, S. W. Cheong, W. Ratcliff, and J. Lynn, *Journal of Physics-Condensed Matter*, 2009, **21**, 456008.
9. I. Kim, Y. S. Oh, Y. Liu, S. H. Chun, J. S. Lee, K. T. Ko, J. H. Park, J. H. Chung, and K. H. Kim, *Applied Physics Letters*, 2009, **94**, 042505.
10. N. Menyuk, K. Dwight, and A. Wold, *Journal de Physique*, 1964, **25**, 528.
11. I. Efthimiopoulos, Z. Liu, S. Khare, V. P. Sarin, T. Lochbiler, V. Tsurkan, A. Loidl, D. Popov, and Y. Wang, *Physical Review B*, 2015, **92**, 064108.
12. Y. Yamasaki, S. Miyasaka, Y. Kaneko, J. P. He, T. Arima, and Y. Tokura, *Physical Review Letters*, 2006, **96**, 207204.
13. R. N. Bhowmik, R. Ranganathan, and R. Nagarajan, *Physical Review B*, 2006, **73**, 144413.
14. D. Zakutna, A. Repko, I. Matulkova, D. Niznansky, A. Ardu, C. Cannas, A. Mantlikova, and J. Vejpravova, *Journal of Nanoparticle Research*, 2014, **16**, 2251.
15. C. Rath and P. Mohanty, *Journal of Superconductivity and Novel Magnetism*, 2011, **24**, 629.
16. C. Rath, P. Mohanty, and A. Banerjee, *Journal of Magnetism and Magnetic Materials*, 2011, **323**, 1698.
17. D. Kumar, J. Galivarapu, A. Banerjee, K. Nemkovski, Y. Su, and C. Rath, *Nanotechnology*, 2016, **27**, 175702.
18. D. Kumar, P. Mohanty, V. Singh, J. K. Galivarapu, A. Banerjee, V. Ganesan, and C. Rath, *Materials Research Bulletin*, 2014, **54**, 78.
19. J. Chen, X. Zhang, H. Arandiyani, Y. Peng, H. Chang, and J. Li, *Catalysis Today*, 2013, **201**, 12.
20. Y. Wang, P. Yang, G. Liu, L. Xu, M. Jia, W. Zhang, and D. Jiang, *Catalysis Communications*, 2008, **9**, 2044.
21. Y. Wang, A. P. Jia, M. F. Luo, and J. Q. Lu, *Applied Catalysis B-Environmental*, 2015, **165**, 477.
22. U. Zavyalova, B. Nigrovski, K. Pollok, F. Langenhorst, B. Mueller, P. Scholz, and B. Ondruschka, *Applied Catalysis B-Environmental*, 2008, **83**, 221.
23. D. P. Dutta, J. Manjanna, and A. Tyagi, *Journal of Applied Physics*, 2009, **106**, 043915.

24. M. Edrisi and A. R. Keshavarz, *Nano-Micro Letters*, 2012, **4**, 83. View Article Online
DOI: 10.1039/C6RA21377D
25. L. Kumar, P. Mohanty, T. Shripathi, and C. Rath, *Nanoscience and Nanotechnology Letters*, 2009, **1**, 199.
26. A. Mantlikova, J. P. Vejpravova, P. Holec, J. Plocek, and D. Niznansky, *IOP Conference Series-Materials Science and Engineering*, 2011, **18**, 032022.
27. H. T. Cui, M. Zayat, and D. Levy, *Journal of Sol-Gel Science and Technology*, 2005, **35**, 175.
28. I. Matulkova, P. Holec, B. Pacakova, S. Kubickova, A. Mantlikova, J. Plocek, I. Nemecek, D. Niznansky, and J. Vejpravova, *Materials Science and Engineering B-Advanced Functional Solid-State Materials*, 2015, **195**, 66.
29. R. K. Singh, A. Yadav, A. Narayan, A. K. Singh, L. Verma, and R. Verma, *Journal of Thermal Analysis and Calorimetry*, 2012, **107**, 197.
30. S. Lei, L. Liu, C. Wang, X. Shen, C. Wang, D. Guo, S. Zeng, B. Cheng, Y. Xiao, and L. Zhou, *Crystengcomm*, 2014, **16**, 277.
31. S. K. Durrani, S. Z. Hussain, K. Saeed, Y. Khan, M. Arif, and N. Ahmed, *Turkish Journal of Chemistry*, 2012, **36**, 111.
32. M. Maczka, M. Ptak, M. Kurnatowska, and J. Hanuza, *Materials Chemistry and Physics*, 2013, **138**, 682.
33. S. Kubickova, J. Plocek, A. Mantlikova, and J. Vejpravova, *Rsc Advances*, 2014, **4**, 5113.
34. J. E. Moses and A. D. Moorhouse, *Chemical Society Reviews*, 2007, **36**, 1249.
35. H. C. Kolb, M. G. Finn, and K. B. Sharpless, *Angewandte Chemie-International Edition*, 2001, **40**, 2004.
36. S. A. McCarthy, G. L. Davies, and Y. K. Gun'ko, *Nature Protocols*, 2012, **7**, 1677.
37. J. Rodriguez-Carvajal and T. Roisnel, *FullProf:98 and WinPLOTR: New Windows 95/NT Applications for Diffraction.Commission for Powder Diffraction, International Union of Crystallography*, 1998.
38. M. K. U. R. Emmanuel Kentzinger, *Journal of large-scale research facilities*, 2016, **2**, A61, <http://dx.doi.org/10.17815/jlsrf-2-109>.
39. W. Schweika and P. Boni, *Physica B-Condensed Matter*, 2001, **297**, 155.
40. X. Wang, J. Zhuang, Q. Peng, and Y. D. Li, *Nature*, 2005, **437**, 121.
41. A. Repko, D. Niznansky, and J. Poltiero-ve-vepravova, *Journal of Nanoparticle Research*, 2011, **13**, 5021.
42. A. Repko, J. Vejpravova, T. Vackova, D. Zakutna, and D. Niznansky, *Journal of Magnetism and Magnetic Materials*, 2015, **390**, 142.
43. M. Bonini, E. Fratini, and P. Baglioni, *Materials Science & Engineering C-Biomimetic and Supramolecular Systems*, 2007, **27**, 1377.
44. J. Preudhom and P. Tarte, *Spectrochimica Acta Part A-Molecular Spectroscopy*, 1971, **A 27**, 1817.
45. Z. V. Popovic, Z. Dohcevic-Mitrovic, M. Scepanovic, M. Grujic-Brojcin, and S. Askrabic, *Annalen der Physik*, 2011, **523**, 62.
46. K. Tomiyasu, J. Fukunaga, and H. Suzuki, *Physical Review B*, 2004, **70**, 214434.
47. C. Zhu, Z. Tian, L. Wang, and S. Yuan, *Journal of Magnetism and Magnetic Materials*, 2015, **393**, 116.
48. Z. Tian, C. Zhu, J. Wang, Z. Xia, Y. Liu, and S. Yuan, *Journal of Magnetism and Magnetic Materials*, 2015, **377**, 176.

49. R. H. Kodama, A. E. Berkowitz, E. J. McNiff, and S. Foner, *Journal of Applied Physics*, 1997, **81**, 5552. [View Article Online](#)
DOI: 10.1039/C6RA21377D
50. J. L. Dormann, D. Fiorani, and E. Tronc, *Advances in Chemical Physics*, 1997, **98**, 283.
51. D. X. Li, S. Nimori, Y. Shiokawa, Y. Haga, E. Yamamoto, and Y. Onuki, *Physical Review B*, 2003, **68**, 012413.
52. S. Shtrikman and E. P. Wohlfarth, *Physics Letters A*, 1981, **85**, 467.
53. J. Souletie and J. L. Tholence, *Physical Review B*, 1985, **32**, 516.



Uniform nanoparticles of multiferroic CoCr_2O_4 dispersible in non-polar solvents were prepared by hydrothermal route in water-alcohol-oleic acid system.